Graphene fractals: Energy gap and spin polarization

Thomas Garm Pedersen [*]

Department of Materials and Production, Aalborg University, DK-9220 Aalborg Øst, Denmark

Graphene is a natural material platform for experimental realization of triangular fractals. Hence, forming triangular holes in the hexagonal lattice following a self-similar recipe leads to fractal Sierpinski triangles. Two subclasses characterized by armchair and zigzag edges are investigated using a mean-field Hubbard approach. We find that zigzag-edged fractals support a significant spin polarization whereas the armchair subclass is spin balanced. Despite this difference, the energy gap between like-spin states is large for both types. A self-similar distribution of energy levels is found in late-generation fractals. In an external magnetic field, the energy gaps tend to decrease, and an intricate dispersion of individual levels is found. This leads to optical Hall conductivities with a seemingly chaotic field dependence in late-generation fractals.

I. INTRODUCTION

Graphene is an exceptional material with a range of excellent properties. The bulk sheets have several useful qualities, such as high carrier mobility and thermal conductance [1]. It has become clear, however, that a key to additional functionalization lies in carefully prepared edges. Thus, extended zigzag edges support spin-polarized states whereas armchair edges are spin balanced. This important difference has been demonstrated in experiments on both graphene nanoribbons and quantum dots [2,3] as well as theory [4,5]. Such spin-polarized edge states could play a role in topologically protected transport and spintronics applications [6,7]. Recently, we have suggested that bulk graphene can be dramatically modified by suitably arranged holes in the sheet, leading to the formation of graphene antidot lattices [8–12]. Hexagonal antidot lattices arranged such that superlattice vectors are parallel to the atomic C-C bonds turn graphene into a semiconductor whereas rotated hexagonal ones may produce both metallic and semiconducting structures [9]. In addition, the edge type of such holes may have dramatic consequences for the magnitude and even existence of a band gap. Thus, holes with extended zigzag edges support edge states within the transport energy gap [10,11]. It has been shown, however, that these states are unstable against spin polarization when electron-electron interactions are accounted for using, e.g., a mean-field Hubbard model [10]. Thus, a gap develops even in this case. Also, antidot lattices with triangular holes and triangular quantum dots are known to support a net spin if edges are predominantly formed by atoms belonging to one of the two graphene sublattices [13]. Hence, graphene-based ferromagnets and spin filters have been envisioned.

Antidot lattices contain a regular pattern of holes forming a periodic structure whose properties are determined by the unit cell. In particular, if only a single hole is formed in each unit cell, this single feature will define all edge states found in the entire sample. In contrast, fractal geometries contain features on all scales. For example, Sierpinski triangles and carpets contain triangular and rectangular holes with sizes doubling for each self-similar generation of the fractal. Sierpinski triangles can be seen as interconnected triangular quantum dots, see Fig. 1. The basic one, shown as generation $g = 1$ in Fig. 1, is reproduced repeatedly in subsequent generations. The maximum size of edges doubles for each generation, however. Hence, structures containing a wide range of edge fragments are formed in high generations. Sierpinski carpets are closely related to triangles but start from a square domain from which squares are removed. From graphene antidot lattices [10], isolated antidots [14], and quantum dots [15], it is known that the size of edge fragments is crucial for the magnetic properties. Hence, it is interesting to see how the scale-invariant distribution of edge segments in fractals determine the magnetic properties of these structures.

In the present paper, triangular Sierpinski fractals based on the graphene lattice are analyzed. In particular, we wish to explore the difference between armchair (AC) and zigzag (ZZ) fractals, designated in this manner after their edge types, see Fig. 1. Graphene-based rectangular Sierpinski carpets [16] and zigzag Sierpinski triangles [17] have previously been analyzed theoretically. However, the geometry analyzed in Ref. [17] is hardly realistic for graphene since basic rules of conjugated molecules are ignored. Thus, hexagons connected by a single carbon atom are included. Consequently, with full hydrogen saturation, two adjacent single bonds breaking the conjugation appear in the fractals analyzed in Ref. [17]. In the present paper, more realistic and fully conjugated models containing only intact hexagons for which edge atoms bind to single hydrogens are considered. Also, in both of the previous cases [16,17], only a simple nearest-neighbor tight-binding model without electron-electron (e-e) interactions was applied. As we demonstrate below, e-e interactions are crucial for a realistic model of ZZ-edged fractals. Thus, we find that, although AC fractals are always gapped, ZZ fractals are
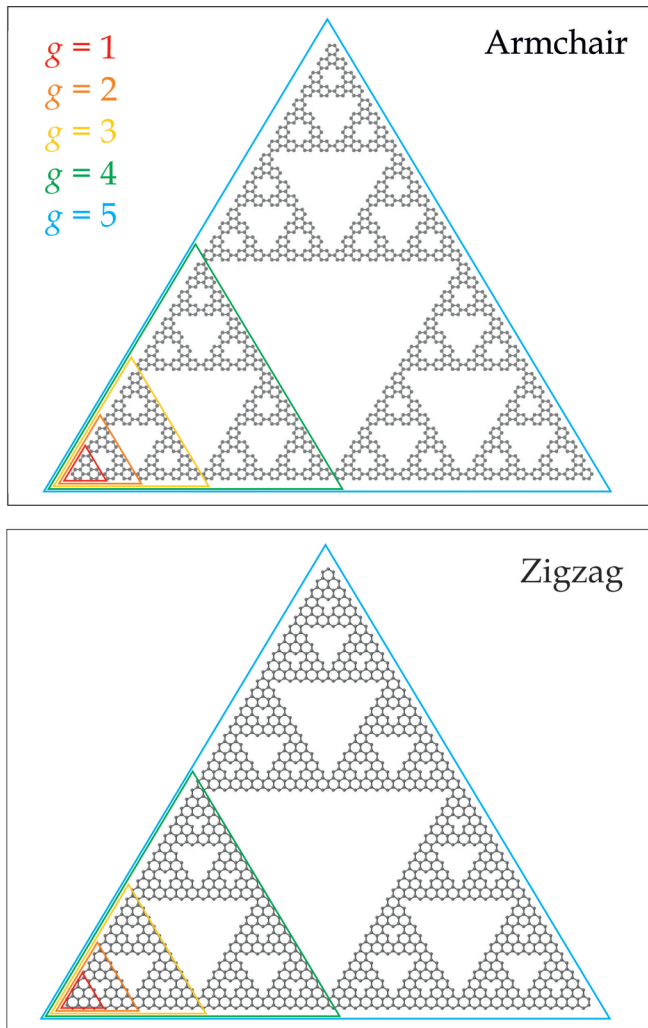
---

[*]tgp@mp.aau.dk

235427-1

FIG. 1. Armchair (top) and zigzag (bottom) graphene fractals with their different generations g indicated by colored triangles.

metallic if e-e interactions are ignored. By adding a mean-field Hubbard interaction, however, the picture changes dramatically. Thus, a pronounced spin polarization emerges leading us to conclude that ZZ fractals are, in fact, gapped ferromagnets. Moreover, if only spin-preserving gaps are considered, these gaps are similar in magnitude to those of the AC type.

Earlier works have presented extensive theoretical studies of Sierpinski fractals based on triangular or quadratic rather than hexagonal lattices. In addition to the pioneering analytical energy spectrum [18], this includes the influence of magnetic fields [19–23] as well as transport properties [24,25], optical response [16], and energy-level statistics [26]. Apart from Sierpinski triangles, these studies also include rectangular Sierpinski carpets [16,23,25]. In the present paper, we examine the influence of external magnetic and optical fields on graphene-based fractals. Using Peierls substitution, magnetic fields are readily incorporated in the mean-field Hubbard model. This leads to a Hofstadter-type energy spectrum, which itself displays fractal features in (energy and flux) space. We then compute the optical response, which directly probes the spin-preserving gap. In the presence of a magnetic field, an off-diagonal optical Hall response emerges.

This response mirrors the fractal character of the energies in magnetic fields. Although no experimental realizations of true graphene fractals exist, we note that geometrically similar structures have been fabricated using CO molecules on surfaces [27], DNA self-assembly [28], and self-assembly of phenyl-based molecules [29–31]. It seems likely that atomically precise bottom-up techniques, such as those developed for nanoribbons [32], could lead to future fabrication of graphene fractals.

II. ELECTRONIC STRUCTURE

We use an orthogonal π-electron tight-binding model to describe the electronic structure of both AC and ZZ fractals. Our previous work on spin-polarized graphene antidot lattices [10] has demonstrated excellent agreement with full density-functional theory provided interactions up to third-nearest neighbors are included. The hopping integrals t_{ij} for first-, second-, and third-nearest neighbors are taken as -2.7, -0.20, and -0.18 eV, respectively. To include electron-electron interactions at the mean-field level, we add an on-site Hubbard U of $U = 2.0$ eV [5,10]. The Hamiltonian is

$$H = \sum_{i,j,\sigma} t_{ij} c_{i\sigma}^\dagger c_{j\sigma} + U \sum_{i,\sigma} \left(n_{i,\bar{\sigma}} - \frac{1}{2} \right) c_{i\sigma}^\dagger c_{i\sigma}. \quad (1)$$

Here, $\sigma \in \{\uparrow, \downarrow\}$ denotes spin, and the first sum is over first-, second-, and third-nearest neighbors whereas the second term is the mean-field Hubbard with $\bar{\uparrow} = \downarrow$ and $\bar{\downarrow} = \uparrow$, i.e., $\bar{\sigma}$ designating the opposite of σ. Also, $c_{i\sigma}$ is the annihilation operator and $n_{i,\sigma} = \langle c_{i\sigma}^\dagger c_{i\sigma} \rangle$ the spin density at atom i and spin σ [the factor $\frac{1}{2}$ subtracted in Eq. (1) amounts to measuring interactions relative to the homogeneously filled case]. Self-consistent eigenstates of Eq. (1) are found by iteration starting from an initial state with uniform spin imbalance. The atomic geometries in Fig. 1 are generated recursively, and the number of atoms is $N_{AC}(g) = 6 \times 3^g$ and $N_{ZZ}(g) = 19 \times 3^{g-1} + 3$ for AC and ZZ, respectively. Thus, the number of atoms is roughly the same for both types at any particular generation g. By inspection, however, it is clear that the geometric difference between AC and ZZ is that, in the latter case, an imbalance between A and B sublattices given by $\Delta N(g) = 2 \times 3^{g-1}$ exists, whereas equal numbers of A and B atoms appear in the AC case. Lieb's theorem [33] states that for a half-filled bipartite lattice with hopping only between A and B atoms, a net spin equal to $\frac{\hbar}{2} \Delta N$ exists at zero temperature. Thus, although our slightly more general model includes hopping within one sublattice (via second-nearest neighbors), significantly different spin properties are expected for AC and ZZ structures as we confirm below.

Focusing first on the AC case, we find a rather robust gapped spectrum. An example of this is shown in Fig. 2(a). As demonstrated in the inset, the gap saturates near a value of $\sim$1.85 eV for large fractals. The reason for the asymmetry between occupied and empty energy eigenvalues is that second-nearest neighbor interactions are included in the model, which would otherwise be electron-hole symmetric. Also, the subgaps near -8 and $+6$ eV are robust features that survive in higher generations. For AC fractals, all levels are twofold spin degenerate and, so, no spin polarization is found
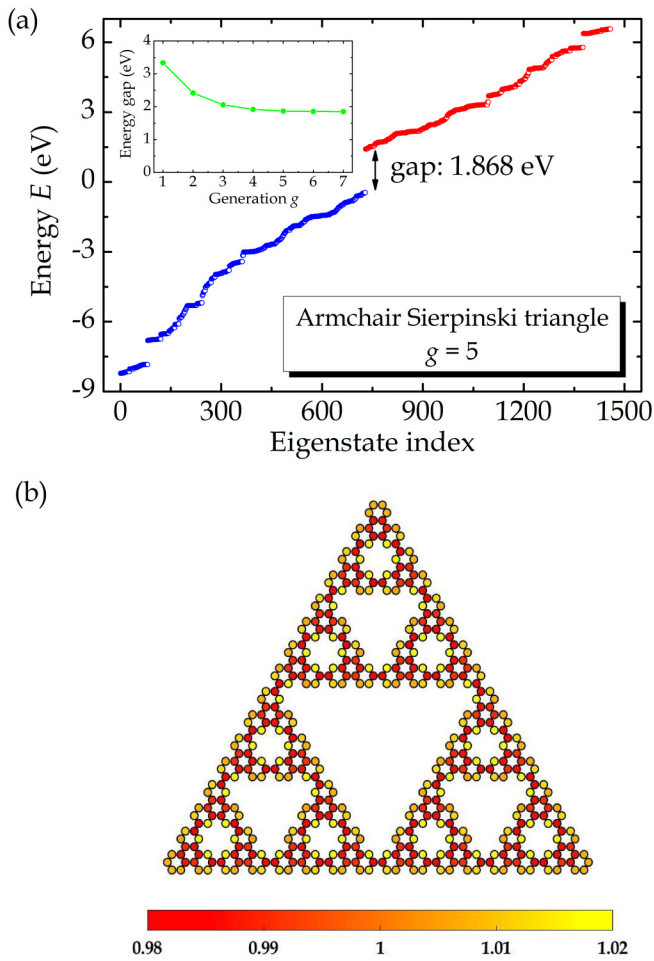
FIG. 2. (a) Energies of all eigenstates for a $g = 5$ AC fractal with Hubbard interaction with occupied and empty states shown in blue and red, respectively. (b) Electron density for $g = 4$. The inset in (a) shows the energy gap versus generation.
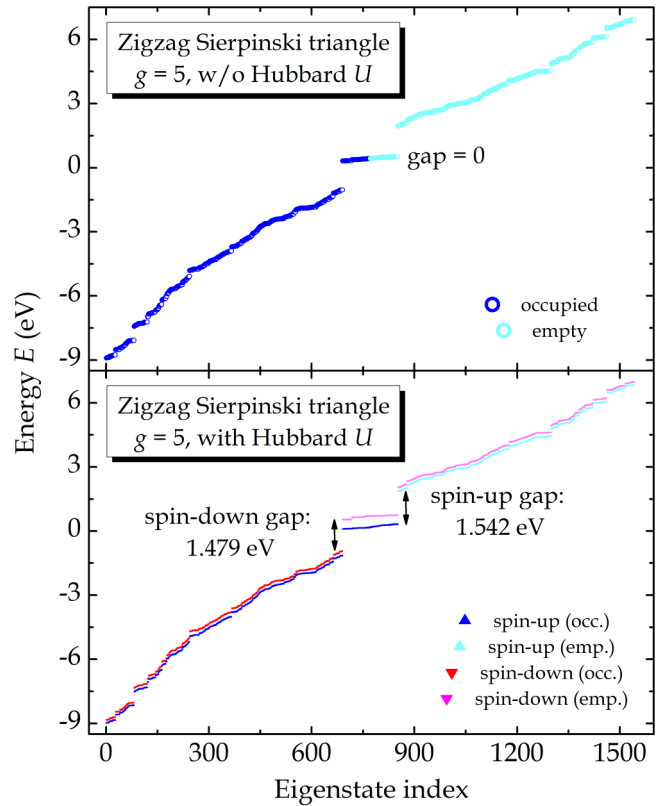

FIG. 3. Energies of a ZZ fractal with $g = 5$. Top and bottom panels show results without and with Hubbard interactions, respectively. Occupied states are shown in blue/red, empty states are shown in cyan/magenta, and the orientation of triangles in the bottom panel designates spin direction.

($n_{i,\uparrow} = n_{i,\downarrow}$). Moreover, the electron density as illustrated in Fig. 2(b) is practically constant having variations only at the 2% level. Hence, to a good approximation $n_{i,\uparrow} = n_{i,\downarrow} \approx 1/2$ leading to an approximately vanishing effect of the Hubbard U term for all levels. In fact, for the case in Fig. 2, the root-mean-square deviation between energies with and without U is only 4 meV.

The ZZ case is significantly more intricate. For these structures, a large fraction of the atoms belong to the same sublattice, cf. Fig. 1. This implies that a large degree of spin polarization is expected. In Fig. 3, we plot the energies of a $g = 5$ ZZ fractal without (top panel) and with (bottom panel) Hubbard interaction. With $U = 0$, there is no penalty for double occupancy of a site and, as a consequence, no spin polarization. In fact, the number of doubly degenerate levels around zero is precisely equal to the number of edge atoms, i.e., 162 for $g = 5$. These states form a close quasicontinuum and, hence, the structure is metallic. This conclusion, however, is drastically altered if electron-electron interactions are included. According to Lieb's theorem [33], the spin imbalance $N_\uparrow - N_\downarrow$ equals the sublattice imbalance ΔN. Hence, for

ZZ fractals, the net spin polarization ζ becomes

$$\zeta = \frac{N_\uparrow - N_\downarrow}{N_\uparrow + N_\downarrow} = \frac{2 \times 3^{g-1}}{19 \times 3^{g-1} + 3} \approx \frac{2}{19}, \qquad (2)$$

where the last approximation is valid for $3^g \gg 1$.

To discuss the behavior of energy gaps versus fractal generation, we consider the highest occupied (HOMO) and lowest unoccupied (LUMO) molecular orbitals for each spin. Three energy gaps exist: a spin-up gap $E_g^\uparrow = E_{\text{LUMO}}^\uparrow - E_{\text{HOMO}}^\uparrow$, a spin-down gap $E_g^\downarrow = E_{\text{LUMO}}^\downarrow - E_{\text{HOMO}}^\downarrow$, and the true gap, which involves flipped spins $E_g = E_{\text{LUMO}}^\downarrow - E_{\text{HOMO}}^\uparrow$. Although the latter is the actual energy gap in the system, the spin-preserving gaps $E_g^\uparrow$ and $E_g^\downarrow$ determine the optical response as optical stimulation to a very good approximation does not induce spin flips in light elements, such as carbon. The dependence of these gaps on generation is shown in Fig. 4(a). Similar to the AC case, the gaps approach their asymptotic values rather closely when $g > 4$ is reached. Moreover, both up and down gaps are about 1.5 eV, which is only slightly less that the AC value of about 1.85 eV. The spin-flipped gap, on the other hand, is much smaller, i.e., $E_g \approx 0.25$ eV. The local spin polarization on the edges is seen to be about $n_\uparrow - n_\downarrow \sim 0.3$ in the inset in Fig. 4(b), and one might naively expect a gap of $U(n_\uparrow - n_\downarrow) \sim 0.6$ eV. However, second-nearest-neighbor coupling leads to a significant
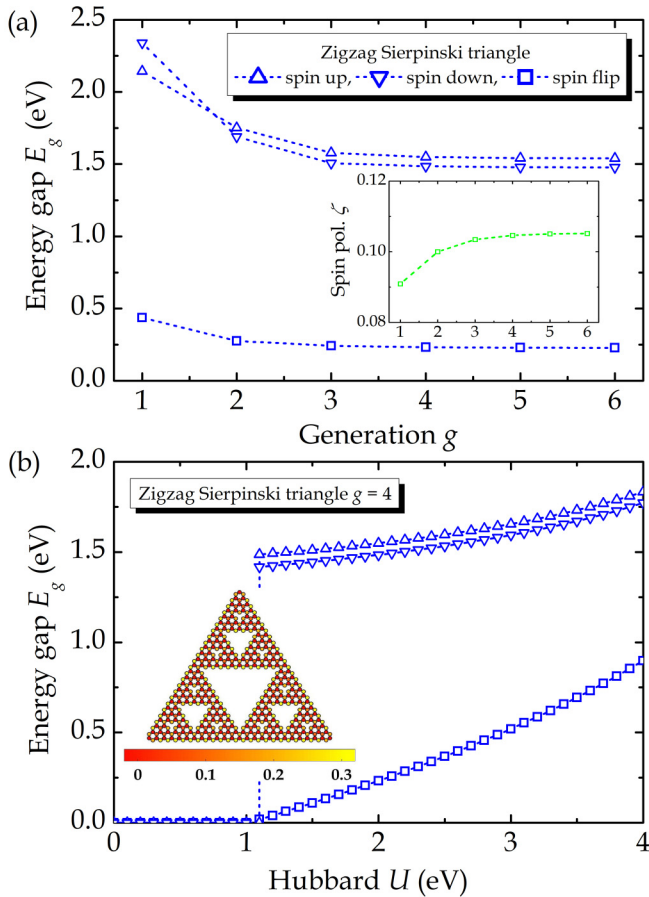
FIG. 4. (a) Spin-preserving and spin-flipped energy gaps for ZZ fractals of different generation g. The inset shows the net spin polarization versus g. (b) Energy gaps versus U for a $g = 4$ ZZ fractal. The inset: local spin-polarization $n_\uparrow - n_\downarrow$ at $U = 2.0$ eV.
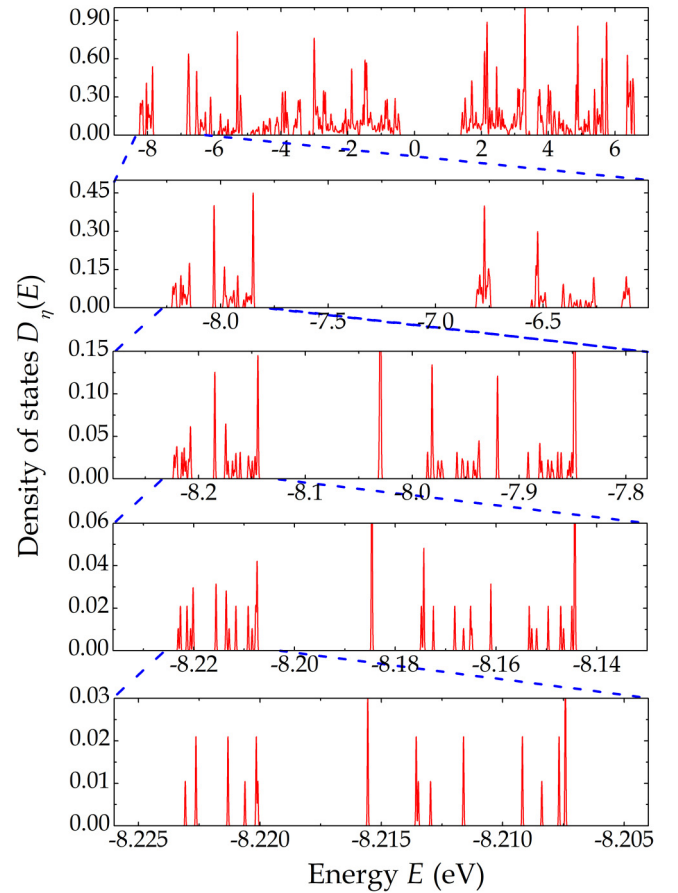

FIG. 5. Repeated zooms of the density of states (normalized by the maximal value) of a $g = 6$ AC fractal. In the four lower panels, energy range and broadening are reduced by factors of 5 in subsequent zooms.

dispersion among the edge states as seen in the central part of Fig. 3 (bottom). Thus, the energy difference between the highest occupied spin-up state (No. 852 for $g = 5$, cf. Fig. 3) and lowest empty spin-down state (No. 691 for $g = 5$) is about half of the naive estimate.

Clearly, the Hubbard U interaction is crucial for a correct model of ZZ fractals. The magnitude of U, however, is not known precisely and should, in principle, also depend on the substrate, on which the sample is placed, due to screening. In the present paper, the value $U = 2.0$ eV is selected from previous comparison with density-functional theory for similar graphene-based structures [5,10]. To study the robustness of our conclusions with respect to the precise value of U, we present the energy gaps versus U for $g = 4$ in Fig. 4(b). Note that $g = 4$ is sufficient to produce energy gaps that are converged with respect to fractal generation. It is seen that a threshold value of $U_c \sim 1.1$ eV is required to produce a finite spin polarization and associated energy gaps. This is a consequence of second-nearest-neighbor hopping coupling atoms within the same sublattice. In the absence of such terms, finite gaps appear at arbitrarily small U as has been verified numerically. Around the applied value of $U = 2.0$ eV, there is little variation of the spin-up and spin-down gaps. The

spin-flipped gap, however, varies nearly linearly with $U - U_c$, and at $U = 3.0$ eV, the value is more than doubled. Therefore, this quantity is quite sensitive to the value of U whereas the spin-preserving gaps are more robust.

Next, we turn to a more precise analysis of the energy-level distribution. It is known [18–20] that levels in simple Sierpinski fractals have a self-similar distribution. We now demonstrate that a similar behavior can be observed in physically realistic graphene fractals. As an example, we focus on a $g = 6$ AC fractal. Self-similarity is revealed by repeatedly zooming into an increasingly narrow energy range [19], such as illustrated in Fig. 5. We add Gaussian broadening to the density of states defined as $D_\eta(E) = \sum_i \exp[-(E - E_i)^2/\eta^2]$. The first panel in Fig. 5 shows the full spectrum, whereas the second is a zoom into a range $E \in [E_0, E_0 + \Delta E]$ with $E_0 = -8.5$ and $\Delta E = 2.5$ eV taking $\eta = 3$ meV. In subsequent zooms, this range is reduced by a fixed factor α, whereas, at the same time, the broadening η is reduced by the same factor. For a Sierpinski triangle, the factor required for self-similarity is $\alpha = 5$ [19]. Thus, in the third panel, $\Delta E = 0.5$ eV whereas $\eta = 0.6$ meV, and so on. The self-similarity is clearly observed, in particular, in the three central panels. For an infinite fractal, self-similarity is sustained
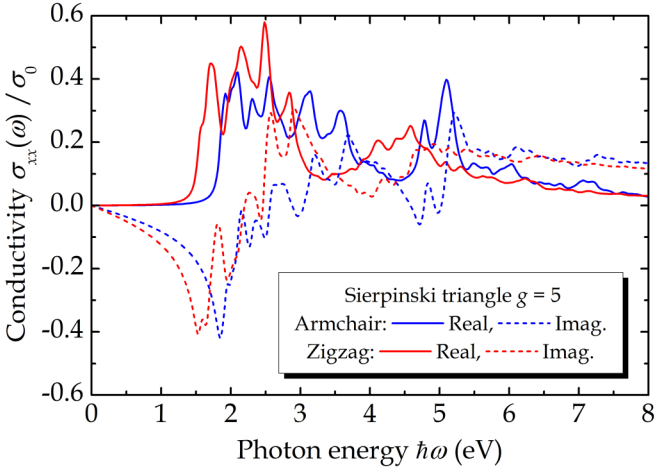
FIG. 6. Real (solid lines) and imaginary (dashed lines) parts of the diagonal optical conductivity for generation $g = 5$ AC (blue) and ZZ (red) fractals.

indefinitely, whereas for finite fractals, self-similarity only survives for a limited number of successive zooms. Nevertheless, the plot demonstrates that physically realistic graphene fractals are expected to host fractally distributed energy levels. This, in turn, will have consequences for, e.g., optical properties of such structures as we show in the following section.

III. OPTICAL AND MAGNETO-OPTICAL PROPERTIES

We now turn to the optical and magneto-optical responses of graphene fractals as examples of the effect of edge type on experimentally accessible quantities. The optical properties are encoded in the frequency- (ω) dependent conductivity,

$$\sigma_{ij}(\omega) = -ie^2\omega \sum_{n,m,\sigma} \frac{f(E_{n\sigma}) - f(E_{m\sigma})}{E_{m\sigma} - E_{n\sigma} - \hbar\omega}$$
$$\times \langle n\sigma | r_i | m\sigma \rangle \langle m\sigma | r_j | n\sigma \rangle, \qquad (3)$$

where $|n\sigma\rangle$ is an eigenstate with energy $E_{n\sigma}$, f is the Fermi-Dirac distribution, and $r_i \in \{x, y\}$ are the spatial coordinates. This form utilizes the connection between current density $\vec{j} = -e\vec{p}/m_e$ and dipole $-e\vec{r}$ matrix elements given by $\langle n\sigma | \vec{p} | m\sigma \rangle = im_e(E_{m\sigma} - E_{n\sigma})\langle n\sigma | \vec{r} | m\sigma \rangle / \hbar$ with m_e as the electron mass and $\vec{p}$ as the momentum operator. The gauge invariance and equivalence between various conductivity formulations are discussed in Ref. [34]. To add line broadening, an imaginary part $i\eta$ with $\eta = 50$ meV is added to the photon energy $\hbar\omega$. Also, a convenient unit of conductivity is $\sigma_0 = e^2 A / \hbar$ with $A = 3^{1/2} a^2 N / 4$ the approximate area of a fractal containing N atoms with a the graphene lattice constant. The fractals are isotropic, and the real part of $\sigma_{xx}(\omega) = \sigma_{yy}(\omega)$ is essentially the optical absorption. In Fig. 6, we show the spectral dependence of the conductivity for both edge orientations taking $g = 5$, which is representative of higher generations also. A large absorption sets in at the spin-preserving energy gap for both AC and ZZ fractals. Moreover, the overall magnitude of the absorption is similar for the two edge types.

In the presence of a magnetic-field B perpendicular to the plane containing the molecules, the hopping integrals

acquire a Peierls phase $t_{ij} \to t_{ij} \exp(i\Phi_{ij}/\Phi_0)$, where $\Phi_0 = \hbar/e$ is the flux quantum and $\Phi_{ij} = \int_{\vec{r}_i}^{\vec{r}_j} \vec{A}(\vec{r}) \cdot d\vec{r}$ the magnetic flux between atomic sites $\vec{r}_{i,j}$ with $\vec{A}(\vec{r})$ the vector potential. In the symmetric gauge, $\Phi_{ij} = \frac{1}{2} B(x_i y_j - y_i x_j)$. Introducing normalized coordinates $x_{i,j} = a\tilde{x}_{i,j}$ and similarly for $y_{i,j}$, one finds $\Phi_{ij}/\Phi_0 = (B/B_0)(\tilde{x}_i \tilde{y}_j - \tilde{y}_i \tilde{x}_j)$ with $B_0 = 2\Phi_0/a^2 \approx 21.6$ kT. Naturally, the magnetic field also couples directly to the spins. This, however, only leads to a rigid shift for all states of the same spin and, as only spin-preserving transitions are probed in the optical response, has no effect as long as fields small enough to preserve the zero-field occupation of states are considered as is the case here. In fact, if only spins are considered, a field of $(E_g^\uparrow + E_g^\downarrow - E_g)/2\mu_B$ is required to switch population between $|\text{HOMO}, \downarrow\rangle$ and $|\text{LUMO}, \uparrow\rangle$ corresponding to $\sim$15 kT for AC fractals and even more for the ZZ case using the zero-field gaps.

In Fig. 7, we present the evolution of energy levels and Hall conductivities σ_{xy} (taking $\eta = 10$ meV to better distinguish transitions) with magnetic field and fractal generation. For clarity, the spin-Zeeman shift is omitted in the energy plots. Concerning the fundamental AC energy gap, a clear shrinkage with field is observed similarly to the antidot lattice case [35]. The same is observed for the gap between dispersive states in ZZ fractals. In contrast, the ZZ edge states remain only weakly perturbed by the magnetic field. The energy levels have a rather intricate dependence on field for the higher generations and, in fact, closer inspection reveals a fractal (in energy-field space) structure, in agreement with the self-similar level distribution found above. Hence, the investigated structures are fractal with respect to both geometry and energy dispersion. A similar fractal dispersion with magnetic field was found for fractals based on triangular lattices in Ref. [20]. The intricate energy-level structure for high g leads to extremely complicated Hall conductivity spectra. Thus, for $g = 2$, the evolution of the spectra with B is smooth but for $g = 4$ appears "chaotic," in particular, for the AC case. This is a consequence of the fact that only relatively large fractals support a highly self-similar energy-level distribution as found in Sec. II. It must be borne in mind, however, that the behavior in Fig. 7 requires extremely large fields and, realistically, the maximal field strength available experimentally is around $\sim$0.01B_0. It would be highly interesting to see this prediction tested in future experimental studies applying, e.g., Faraday rotation to probe graphene fractals. We also note that exceedingly large ($\sim$800-T) pseudomagnetic fields in graphene have been obtained by strain engineering [36]. This may open an alternative route to verification of the resent results.

IV. SUMMARY

We studied the electronic, optical, and magneto-optical properties of graphene-based Sierpinski triangle fractals using a mean-field Hubbard model. Both ZZ- and AC-edged structures were investigated, and significant differences were observed similar to nanoribbons, quantum dots, and antidots. Thus, ZZ Sierpinski triangles feature a large fraction of edge states and asymptotically 2/19 of all atoms are edge sites belonging to a single sublattice for late-generation ZZ
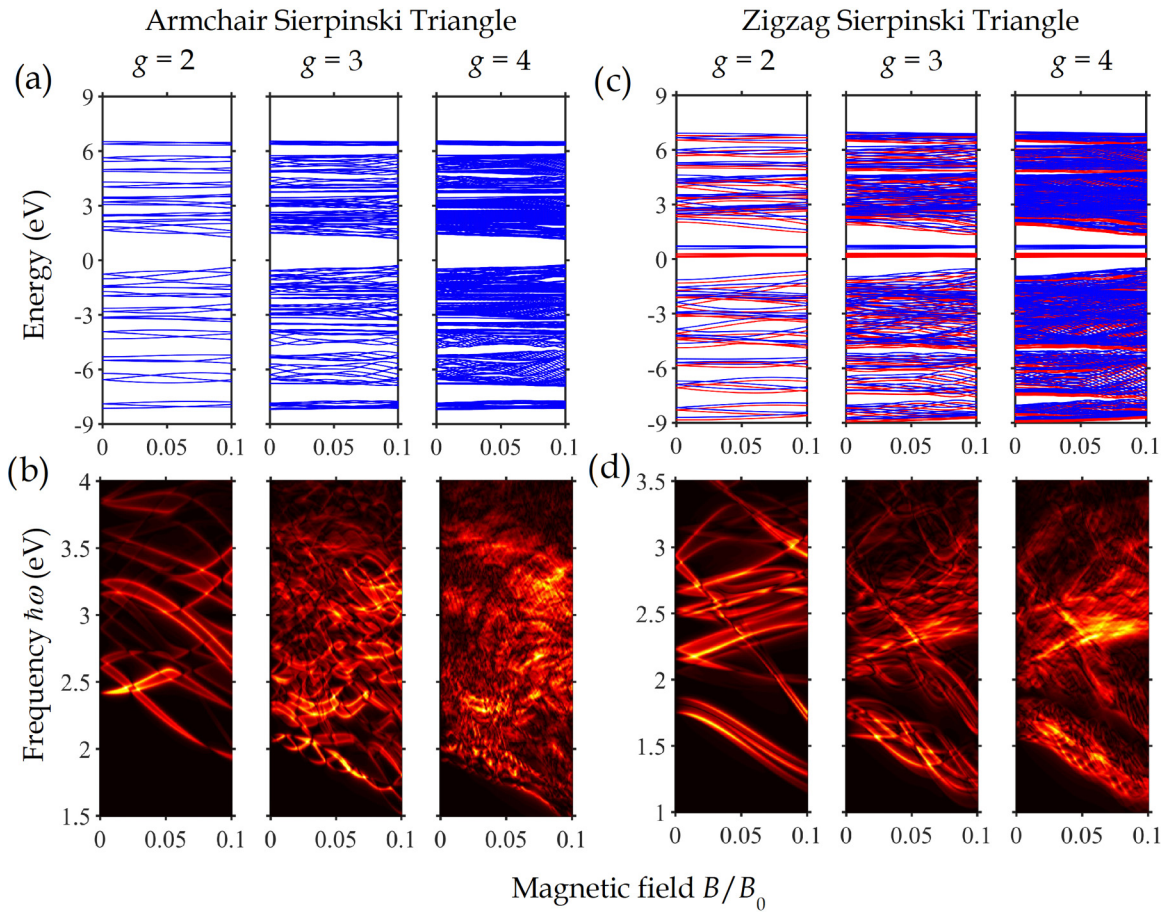
FIG. 7. Effect of a magnetic field on (a) and (c) energy eigenvalues and (b) and (d) Hall conductivity $|\sigma_{xy}(\omega)|$. Panels (a) and (b) are for AC and (c) and (d) for ZZ fractals. In (a), all states are spin degenerate and in (c), red and blue designate spin up and down, respectively. In (b) and (d), lighter colors indicate higher $|\sigma_{xy}|$ values.

fractals. This leads to an instability against spin polarization if electron-electron interaction is taken into account. In contrast, AC-edged fractals remain spin balanced. In both cases, a large spin-preserving energy gap is predicted. This leads to pronounced optical absorption in the visible energy range. The distribution of energy levels is shown to be self-similar for late-generation fractals. As a consequence, an intricate pattern emerges leading to a seemingly chaotic behavior of the optical Hall conductivity.

[1] A. H. Castro Neto, F. Guinea, N. M. R. Peres, K. S. Novoselov, and A. K. Geim, Rev. Mod. Phys. **81**, 109 (2009).

[2] G. Z. Magda, X. Jin, I. Hagymási, P. Vancsó, Z. Osváth, P. Nemes-Incze, C. Hwang, L. P. Biró, and L. Tapasztó, Nature (London) **514**, 608 (2014).

[3] Y. Sun, Y. Zheng, H. Pan, J. Chen, W. Zhang, L. Fu, K. Zhang, N. Tang, and Y. Du, npj Quantum Mater. **2**, 5 (2017).

[4] Y.-W. Son, M. L. Cohen, and S. G. Louie, Phys. Rev. Lett. **97**, 216803 (2006).

[5] Y. Hancock, A. Uppstu, K. Saloriutta, A. Harju, and M. J. Puska, Phys. Rev. B **81**, 245402 (2010).

[6] W. Sheng, Z. Y. Ning, Z. Q. Yang, and H. Guo, Nanotechnology **21**, 385201 (2010).

[7] X. H. Zheng, G. R. Zhang, Z. Zeng, V. M. García-Suárez, and C. J. Lambert, Phys. Rev. B **80**, 075413 (2009).

[8] T. G. Pedersen, C. Flindt, J. Pedersen, N. A. Mortensen, A.-P. Jauho, and K. Pedersen, Phys. Rev. Lett. **100**, 136804 (2008).

[9] R. Petersen, T. G. Pedersen, and A.-P. Jauho, ACS Nano **5**, 523 (2011).

[10] M. L. Trolle, U. S. Møller, and T. G. Pedersen, Phys. Rev. B **88**, 195418 (2013).

[11] S. J. Brun, M. Thomsen, and T. G. Pedersen, J. Phys.: Condens. Matter **26**, 265301 (2014).

[12] B. S. Jessen, L. Gammelgaard, M. R. Thomsen, D. M. A. Mackenzie, J. D. Thomsen, J. M. Caridad, E. Duegaard, K. Watanabe, T. Taniguchi, T. J. Booth, T. G. Pedersen, A.-P. Jauho, and P. Bøggild, Nat. Nanotechnol. **14**, 340 (2019).

[13] S. S. Gregersen, S. R. Power, and A.-P. Jauho, Phys. Rev. B **95**, 121406(R) (2017).

[14] M. R. Thomsen and T. G. Pedersen, Phys. Rev. B **95**, 235427 (2017).

[15] W. L. Wang, S. Meng, and E. Kaxiras, Nano Lett. **8**, 241 (2008).

[16] E. van Veen, S. Yuan, M. I. Katsnelson, M. Polini, and A. Tomadin, Phys. Rev. B **93**, 115428 (2016).

[17] H. Yorikawa, J. Phys. Commun. **3**, 085004 (2019).

[18] R. Rammal and G. Toulouse, Phys. Rev. Lett. **49**, 1194 (1982).

[19] E. Domany, S. Alexander, D. Bensimon, and L. P. Kadanoff, Phys. Rev. B **28**, 3110 (1983).

[20] J. M. Ghez, Y. Y. Wang, R. Rammal, B. Pannetier, and J. Bellissard, Solid State Commun. **64**, 1291 (1987).

[21] A. Chakrabarti and B. Bhattacharyya, Phys. Rev. B **56**, 13768 (1997).

[22] Y. Liu, Z. Hou, P. M. Hui, and W. Sritrakool, Phys. Rev. B **60**, 13444 (1999).

[23] M. Brzezińska, A. M. Cook, and T. Neupert, Phys. Rev. B **98**, 205116 (2018).

[24] Z. Lin, Y. Cao, Y. Liu, and P. M. Hui, Phys. Rev. B **66**, 045311 (2002).

[25] E. van Veen, A. Tomadin, M. Polini, M. I. Katsnelson, and S. Yuan, Phys. Rev. B **96**, 235438 (2017).

[26] A. A. Iliasov, M. I. Katsnelson, and S. Yuan, Phys. Rev. B **99**, 075402 (2019).

[27] S. N. Kempkes, M. R. Slot, S. E. Freeney, S. J. M. Zevenhuizen, D. Vanmaekelbergh, I. Swart, and C. Morais Smith, Nat. Phys. **15**, 127 (2019).

[28] P. W. K. Rothemund, N. Papadakis, and E. Winfree, PLOS Biol. **2**, e424 (2004).

[29] J. Shang, Y. Wang, M. Chen, J. Dai, X. Zhou, J. Kuttner, G. Hilt, X. Shao, J. M. Gottfried, and K. Wu, Nat. Chem. **7**, 389 (2015).

[30] H. Wang, X. Zhang, Z. Jiang, Y. Wang, and S. Hou, Phys. Rev. B **97**, 115451 (2018).

[31] Y. Mo, T. Chen, J. Dai, K. Wu, and D. Wang, J. Am. Chem. Soc. **141**, 11378 (2019).

[32] J. Cai, P. Ruffieux, R. Jaafar, M. Bieri, T. Braun, S. Blankenburg, M. Muoth, A. P. Seitsonen, M. Saleh, X. Feng, K. Müllen, and R. Fasel, Nature (London) **466**, 470 (2010).

[33] E. H. Lieb, Phys. Rev. Lett. **62**, 1201 (1989).

[34] A. Taghizadeh, F. Hipolito, and T. G. Pedersen, Phys. Rev. B **96**, 195413 (2017).

[35] J. G. Pedersen and T. G. Pedersen, Phys. Rev. B **87**, 235404 (2013).

[36] C.-C. Hsu, M. L. Teague, J.-Q. Wang, and N.-C. Yeh, Sci. Adv. **6**, eaat9488 (2020).